Light scattering from magnetic excitations in orthoferrites

R. M. White, R. J. Nemanich, and Conyers Herring*
Xerox Palo Alto Resarch Centers, Palo Alto, California 94304
(Received 6 July 1981)

The Raman spectra of $YFeO_3$, $SmFeO_3$, $DyFeO_3$, $HoFeO_3$, and $ErFeO_3$ have been measured as a function of temperature from 8 to 650 K. For all the materials, the spectra show two features in the 5 to 20 cm^{-1} range. From their polariziation properties, these two modes are identified as the two predicted spin-wave modes. For several of the samples, the ratio of the intensity of the Stokes-shifted to anti-Stokes-shifted peaks is not as expected for boson excitations. In addition, rotating the sample by 90° causes an inversion of the Stokes–to–anti-Stokes intensity ratio. The effect has been attributed to an intereference between linear and quadratic magnetic contributions to the dielectric function, and this model can account for the observations. Another striking effect probed by the light scattering is the spin-reorientation transition which occurs in the vicinity of 470 and 90 K for $SmFeO_3$ and $ErFeO_3$, respectively. In this transition, the net magnetic moment rotates continuously by 90° in the *ac* plane, with a resultant change in the spin-wave symmetries. This transition occurs over a temperature interval of about 20 K, during which the frequency of one of the spin-wave modes is expected to go to zero. While the change in spin-wave symmetry is reflected in the light scattering spectra, we do not observe complete "softening," and attribute this observation to a coupling with the rare-earth electronic states.

I. INTRODUCTION

The rare-earth orthoferrites, $RFeO_3$, are a well-studied family of magnetic materials with a rich array of magnetic properties.[1] The orthoferrites are particularly interesting because of the presence of an antisymmetric exchange interaction which involves the vector cross product of neighboring spins as opposed to the usual scalar product. In the absence of this interaction, the orthoferrites would be antiferromagnets. Its presence leads to a small canting of the sublattices making the orthoferrites "weak" ferromagnets with $4\pi M \simeq 100$ Oe. Another interesting feature of these materials is the fact that some of them exhibit a transition as a function of temperature in which the direction of the net magnetization rotates by 90°.

Since yttrium is nonmagnetic, studies of $YFeO_3$ enable one to selectively investigate the magnetic interactions between the Fe^{3+} ions. Before growth-induced anisotropy was discovered in the rare-earth garnets, the orthoferrites were used in magnetic bubble devices. However, the small magnetization results in relatively large bubble sizes. On the other hand, domain-wall mobilities can be very high, particularly in $YFeO_3$. Because of this high mobility, $YFeO_3$ was chosen as the material for an earlier investigation[2] of domain wall motion. One of the outcomes of this investigation was a calculation of the spin-wave frequencies and lifetimes in $YFeO_3$. The spin-wave spectrum consists of two branches. The $\vec{k}=0$ modes correspond to ferromagnetic- and antiferromagneticlike resonances. The frequencies of these modes, based on parameters obtained from susceptibility, etc., are predicted to fall in the far infrared. However, the anisotropy parameters are numerous and difficult to evaluate from static measurements. Although inelastic neutron scattering measurements have been carried out on several rare-earth orthoferrites, we are not aware of such direct determinations of the resonance frequencies in $YFeO_3$. In this paper, we report on Raman scattering measurements on $YFeO_3$ as well as several other orthoferrites from which we obtain the resonance frequencies. A preliminary report of the room-temperature results was presented earlier.[3] The Raman scattering in these materials revealed a number of interesting features some of which have their origin in the magnetic symmetry of the crystals. In Sec. II, we present a group-theoretical analysis of $YFeO_3$ from which the symmetries of the Raman tensor and the dielectric tensor are obtained. A microscopic interpretation of these results is also presented. Section III describes the experimental results. Of particular interest was the observation that the spin-wave frequencies do not "soften" completely at the spin reorientation.

II. THEORY

A. Magnetic group

The crystal structure[4] of $YFeO_3$ is shown in Fig. 1. Not shown in this figure is the fact that the yttrium

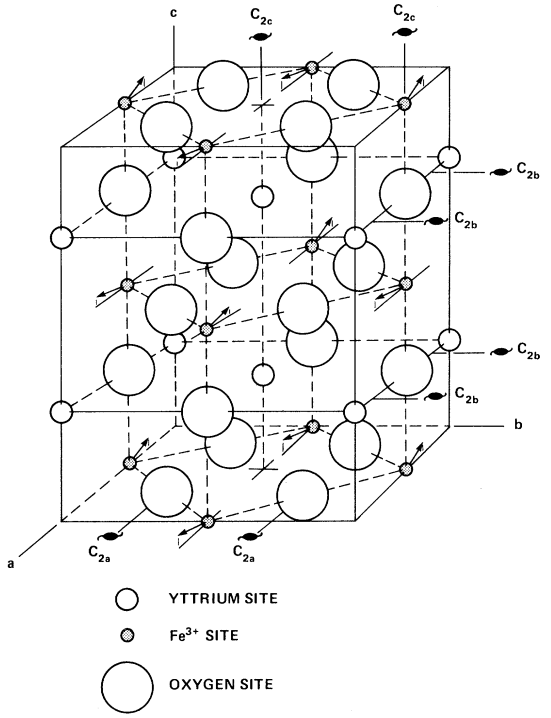

FIG. 1. Unit cell of yttrium orthoferrite.

ions are displaced slightly. The ion at $1\,0\,\frac{1}{4}$ for example, actually lies at $1-x\,-y\,\frac{1}{4}$ while that at $1\,0\,\frac{3}{4}$ lies at $1+x\;y\;\frac{3}{4}$ where x and y are small. This structure belongs to the orthorhombic space group *Pnma* in the international notation, or D_{2h}^{16} in the Schoenflies notation. The symmetry elements in this (unitary) group, let us denote it $\underline{G}$, are as follows:

$\{E|0\}$, the identity operator;

$\{C_{2a}|a/2\}$, $\{C_{2b}|b/2\}$, $\{C_{2c}|c/2\}$: rotations through 180° about the axes indicated in Fig.1 plus a transition by half the repeat distance along that axis (note that we have used different coordinate origins for these three rotations);

$\{I|0\}$ inversion about an Fe^{3+} site;

$\{\sigma_a|b/2\} = \{C_{2b}|b/2\}\cdot\{I|0\}$, reflection in a plane at $a/4$ or $3a/4$ plus a translation along the b axis by $b/2$;

$\{\sigma_b|a/2\} = \{C_{2a}|a/2\}\cdot\{I|0\}$, reflection in a plane at $b/4$ or $3b/4$ plus a translation along the a axis by $a/2$;

$\{\sigma_c|c/2\} = \{C_{2c}|c/2\}\cdot\{I|0\}$, reflection in a plane at $c/4$ or $3c/4$ plus a translation along the c axis by $c/2$;

and combinations of these with lattice translations. These operations leave the charge density invariant. If we wish to consider the magnetic moments we must include the time-reversal operator, T. The full (nonunitary) space group $\underline{M}$ of the *nonmagnetic* crystal then becomes $\underline{M} = \underline{G} + T\underline{G}$, and would be denoted *Pnma* 1′. The ordered magnetic state is *not* invariant under time reversal. Therefore, the space group appropriate for the magnetically ordered system must necessarily be a subgroup of $\underline{M}$. There are eight such subgroups. The one that characterizes the spin configuration shown in Fig. 1 is *Pn′m′a*, whose associated point group we shall describe in the next paragraph.

We shall restrict our considerations to one-magnon scattering. Two-magnon scattering will have a continuous spectrum overlapping that of the phonon bands. The restriction to single magnons simplifies matters, since, at small wave vectors, the symmetry properties can be described in terms of the magnetic *point* group. This is obtained from the space group by setting all the translations, both primitive and nonprimitive, to zero. The resulting magnetic point group, let us denote it by M, is $m'm'm$;

$$M = \{E, I, C_{2z}, \sigma_z, TC_{2x}, TC_{2y}, T\sigma_x, T\sigma_y\} \quad . \tag{1}$$

Half of the elements of M constitute a subgroup of unitary operators, u_i, called the halving subgroup, H, while the other half is a set of antiunitary operators, a_j. Thus, $M = H + T(G-H)$, where G is the point group obtained from $\underline{G}$. From the elements of $\underline{G}$, we see that G is *mmm* (or D_{2h}). The halving subgroups H have been worked out for the 58 magnetic point groups and are tabulated in several places.[5] In the case of $m'm'm$, the unitary subgroup H is $2/m$ (or C_{2h}). The elements of this group, which should be obvious from Eq. (1), and their representations are given in Table I. The antiunitary co-set, $T(G-H)$, may also be written a_0H, where a_0 is any one of the antiunitary elements

The transformation properties of antiunitary groups are characterized by their co-representations. The procedure for finding these co-representations in

TABLE I. Irreducible representation of the halving subgroup H which, in this case, is $2/m$ (or C_{2h}).

$\Delta(u_i)$ \ u_i	E	I	C_{2z}	σ_z
A_g	1	1	1	1
A_u	1	−1	1	−1
B_g	1	1	−1	−1
B_u	1	−1	−1	1

TABLE II. Real co-representations of the magnetic point group $m'm'm$.

$a_0 = TC_{2x}$	E	I	C_{2z}	σ_z	TC_{2x}	$T\sigma_x$	TC_{2y}	$T\sigma_y$	
A_g	1	1	1	1	1	1	1	1	M_z, x^2, y^2, z^2
$\underline{A}_g$	1	1	1	1	−1	−1	−1	−1	$xy, M_x M_y$
A_u	1	−1	1	−1	1	−1	1	−1	
$\underline{A}_u$	1	−1	1	−1	−1	1	−1	1	z
B_g	1	1	−1	−1	1	1	−1	−1	M_y, yz
$\underline{B}_g$	1	1	−1	−1	−1	−1	1	1	M_x, xz
B_u	1	−1	−1	1	1	−1	−1	1	x
$\underline{B}_u$	1	−1	−1	1	−1	1	1	−1	y

terms of the representations of the unitary subgroup was developed by Wigner.[6] Suppose $\Delta(u_i)$ is a unitary irreducible representation of H. Then we first form $\bar{\Delta}(u_i)$ which is defined as

$$\bar{\Delta}(u_i) = \Delta(a_0^{-1} u_i a_0)^* \ , \tag{2}$$

where a_0 is again any one of the antiunitary elements. If $\bar{\Delta}(u_i)$ and $\Delta(u_i)$ are *equivalent, that is, if* $\bar{\Delta}(u_i)$ *may be written as* $\beta^{-1}\Delta(u_i)\beta$, where β is some unitary transformation, then there are two types of co-representations. If $\beta^*\beta = +\Delta(a_0^2)$, then

$$\begin{aligned} D(u_i) &= \Delta(u_i) \ , \\ D(a_i) &= \Delta(a_i a_0^{-1})\beta \ . \end{aligned} \tag{3}$$

If $\beta^*\beta = -\Delta(a_0^2)$, then

$$\begin{aligned} D(u_i) &= \begin{pmatrix} \Delta(u_i) & 0 \\ 0 & \Delta(u_i) \end{pmatrix} , \\ D(a_i) &= \begin{pmatrix} 0 & \Delta(a_i a_0^{-1})\beta \\ -\Delta(a_i a_0^{-1})\beta & 0 \end{pmatrix} . \end{aligned} \tag{4}$$

If $\bar{\Delta}(u_i)$ is *not* equivalent to $\Delta(u_i)$, then the co-representations are of the third type:

$$\begin{aligned} D(u_i) &= \begin{pmatrix} \Delta(u_i) & 0 \\ 0 & \bar{\Delta}(u_i) \end{pmatrix} , \\ D(a_i) &= \begin{pmatrix} 0 & \Delta(a_i a_0) \\ \Delta(a_0^{-1} a_i)^* & 0 \end{pmatrix} . \end{aligned} \tag{5}$$

Notice that a_0 is our case may be written as Tu_0 where u_0 is the appropriate member of G-H. Thus, $a_0^{-1} u_0 a_0 = u_0^{-1} u_i u_0$. But the representations of G are all one dimensional. Therefore, $u_0^{-1} u_i u_0 = u_i$ and $\bar{\Delta}(u_i) = \Delta(u_i)$. From observation, we see that $\bar{\Delta}(u_i)$ may be written as $\beta^{-1}\Delta(u_i)\beta$, where $\beta = \exp(i\theta)$ with θ arbitrary. We then have $\beta^*\beta = +\Delta(a_0^2)$ since $a_0^2 = E$, so the co-representations are of the first type. For the classification of quantum states, for which a change of complex phase has no physical meaning, the possible co-representations can thus be labeled as in Table I, with an arbitrary phase of β assignable to each. For the classification of classical tensors like the susceptibility, for which the real and imaginary parts have different physical meanings, it is convenient to consider co-representations consisting only of real matrices, and thus to distinguish the two cases $\beta = \pm 1$, i.e., to distinguish two alternatives for each row of Table I, as shown in Table II.

B. Spin-wave symmetries

The spin waves, being normal modes of the system, must transform according to the irreducible co-representations developed in Sec. II A. We shall discuss these modes in terms of the two-sublattice model of $YFeO_3$ shown in Fig. 1, in which the spins of all the Fe atoms that point in the same direction are assumed to move together. This model has a single isotropic exchange constant coupling nearest-neighbor Fe spins, a single antisymmetric (canting) exchange constant, and two anisotropy constants; Herrmann[7] has shown that one gets essentially identical results from a more general four-sublattice model with neighbors at different distances allowed to have slightly different couplings, and with slightly different anisotropies for the different sublattices. Thus we write the Hamiltonian

$$\begin{aligned} \underline{H} = 2J \sum_{nn} \vec{S}_i \cdot \vec{S}_j + D \sum_{nn} (S_i^z S_j^x - S_i^x S_j^z) \\ - K_x \left[\sum_i (S_i^x)^2 + \sum_j (S_j^x)^2 \right] \\ - K_z \left[\sum_i (S_i^z)^2 + \sum_j (S_j^z)^2 \right] , \end{aligned} \tag{6}$$

where J (equal to 40.2 cm^{-1}) is the isotropic exchange and D (equal to 0.88 cm^{-1}) is the antisymmetric exchange. The anisotropy constants K_x and K_z correspond to fields of 996 and 245 Oe, respec-

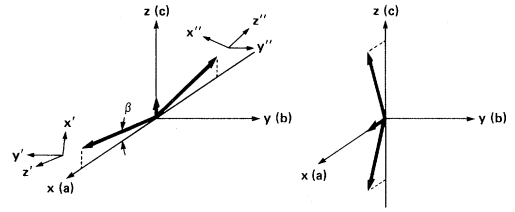

FIG. 2. Two of the allowed spin configurations compatible with the symmetry of the orthoferrites.

tively, as determined by our Raman results at room temperature. These values lead to an equilibrium-canted spin configuration in which the spins lie in xz plane with their net moment along the z axis as illustrated in Fig. 2 (left). This configuration is denoted $\Gamma_4(F_z)$. There are two spin-wave modes which we label σ and γ. The $k=0$ frequencies are[2,7]

$$\hbar\omega_\sigma = [24JS[2(K_x-K_z)S]]^{1/2} ,$$
$$\hbar\omega_\gamma = [24JS(6DS\tan\beta+2K_xS)]^{1/2} , \tag{7}$$

where β is the canting angle. The spin-wave eigenvalues and eigenfunctions were derived in Ref. 2. The $\vec{k}=0$ modes are illustrated in Fig. 3. In order to determine how these modes transform, we must determine the effect of each element of M on these

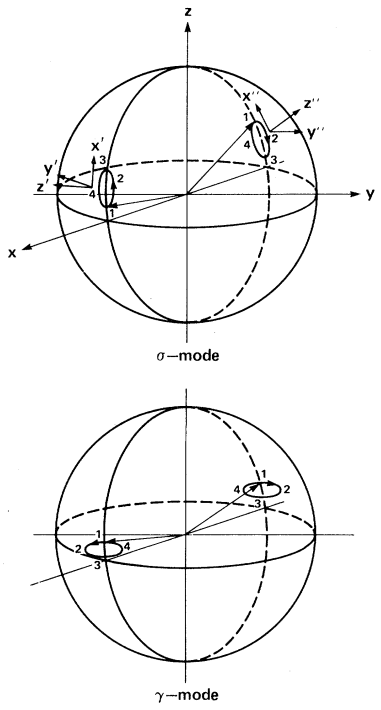

FIG. 3. Precessional motion of the two $k=0$ spin-wave modes.

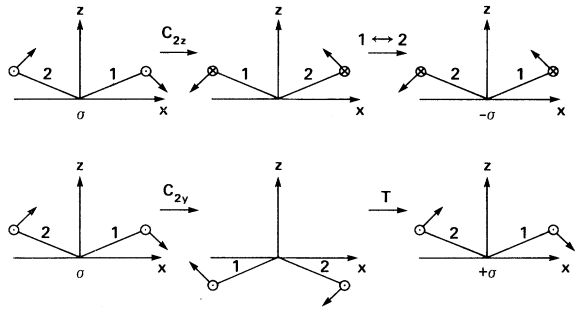

FIG. 4. An illustration of the effects of certain symmetry operations on the σ mode. The lines labeled 1,2 designate the static equilibrium orientations of the two sublattice moments. A complex normal-mode coordinate (spin deviation) is indicated with its real part represented by the arrows in the plane of the drawing and its imaginary part normal to this plane and directed upward (○) or downward (⊕).

configurations. Consider, for example, the action of C_{2z} on the σ mode. This is illustrated at the top of Fig. 4. In order to compare the result with the original configuration, we must also make a site interchange. We end up with the same rocking mode, but it is now 180° out of phase. Thus, $C_{2y}\sigma=-\sigma$. Similarly, the bottom of Fig. 4 shows that $TC_{2y}\sigma=+\sigma$. In this case, since the rotation takes atoms of each sublattice into atoms of the same sublattice, no site interchange is necessary. Notice also that in determining the effect of time reversal, we must not only reverse the direction of the spin but also that of the applied field which governs the direction of precession. As time progresses, the mode will precess back into itself. Thus, a spin-wave mode is characterized by a co-representation of Table I or a pair from Table II. Proceeding in this manner, we find that σ transforms into plus or minus itself. In particular, we find that σ transforms according to B_g and $\underline{B}_g$. Similarly, γ transforms according to A_g and $\underline{A}_g$.

C. Symmetry of the Raman tensor

The Raman scattering cross section is proportional to

$$\left|\sum_{\mu,\nu} E^{\nu}_{\text{out}} R_{\mu\nu} E^{\mu}_{\text{in}}\right|^2 ,$$

where E^{μ}_{in} is the electric field component in the μth direction associated with the incident light, while E^{ν}_{out} refers to the scattered light. $R_{\mu\nu}$ is a tensor of rank two which belongs to a co-representation of M; it is complex in general, though only the relative phases of its different components are physically significant. The Raman tensors for the 58 magnetic point groups have been worked out and tabulated by Cracknell.[8]

For $m'm'm$

$$R(A_g,\underline{A}_g)=\begin{pmatrix} A & iB & 0 \\ iD & E & 0 \\ 0 & 0 & I \end{pmatrix}, \tag{8}$$

$$R(B_g,\underline{B}_g)=\begin{pmatrix} 0 & 0 & iC \\ 0 & 0 & F \\ iG & H & 0 \end{pmatrix}, \tag{9}$$

where A, B, etc., are constants that depend upon microscopic considerations.

Since the Raman tensor reflects the symmetry of the mode excited, we conclude that the Raman tensor associated with the σ mode should have the form (9), while that associated with the γ mode should have the form (8). We notice, in particular, that these modes should not appear in the same polarization.

D. Dielectric function

The Raman tensor is the derivative of the dielectric function with respect to the excited mode amplitude. We can gain additional information about the Raman tensor by considering thet dielectric tensor, $\epsilon_{\alpha\beta}$, itself. This tensor is complex and, if the medium is dissipative, the components will also have anti-Hermitian parts, i.e.,

$$\epsilon_{\alpha\beta}=([\epsilon^H_{\alpha\beta}]'+[\epsilon^A_{\alpha\beta}]')+i([\epsilon^H_{\alpha\beta}]''+[\epsilon^A_{\alpha\beta}]'') \ . \tag{10}$$

The magnetization-dependent contribution to the dielectric tensor, $\Delta\epsilon_{\alpha\beta}$, will be a function of the sublattice magnetizations. We shall develop it to the second order in these magnetizatons, and then consider its first-order increment when the magnetizations depart slightly from their equilibrium values. Since the operations C_{2z}, σ_z, TC_{2x}, and $T\sigma_x$ interchange the sublattices, it is appropriate to expand $\Delta\epsilon_{\alpha\beta}$ in terms of the sums and differences of the sublattice moments. Only those terms having the appropriate symmetry will occur in the various components. In the Appendix we establish the general formalism for determing the symmetry of any response function and apply it specifically to the dielectric function. The symmetries of the various components are listed in Table III. In Table IV, we list the symmetries of the various combinations of sublattice moments. From these tables, we find

$$[\Delta\epsilon^H_{xy}]'+i[\Delta\epsilon^A_{xy}]''=K_{xyy}(M_{1y}-M_{2y})+\ldots \ ,$$

$$i[\Delta\epsilon^H_{xy}]''+[\Delta\epsilon^A_{xy}]'=K_{xyx}(M_{1x}-M_{2x})+K_{xyz}(M_{1z}+M_{2z})+\ldots \ ,$$

where the ellipses represent terms of second order in the M's, and the K's are coefficients describing the optical response of a single ion. Since $[\Delta\epsilon^H_{xy}]'$ and $[\Delta\epsilon^A_{xy}]''$ are symmetric with respect to x and y, we also have

$$[\Delta\epsilon^H_{yx}]'+i[\Delta\epsilon^A_{yx}]''=K_{xyy}(M_{1y}-M_{2y})+\ldots \ .$$

But the Onsager relation requires that $\epsilon_{yx}(-M)=\epsilon_{xy}(M)$; therefore $K_{xyy}=0$. It is straightforward to apply these arguments to the other components and

TABLE III. Symmetries of the various components of the Hermitian and anti-Hermitian parts of the dielectric tensor.

Components	Representations
$[\epsilon^H_{\alpha\alpha}]'+i[\epsilon^A_{\alpha\alpha}]''$	A_g
$[\epsilon^H_{xy}]'+i[\epsilon^A_{xy}]''$	$\underline{A}_g$
$[\epsilon^A_{xy}]'+i[\epsilon^H_{xy}]''$	A_g
$[\epsilon^H_{xz}]'+i[\epsilon^A_{xz}]''$	$\underline{B}_g$
$[\epsilon^A_{xz}]'+i[\epsilon^H_{xz}]''$	B_g
$[\epsilon^H_{yz}]'+i[\epsilon^A_{yz}]''$	B_g
$[\epsilon^A_{yz}]'+i[\epsilon^H_{yz}]''$	$\underline{B}_g$

TABLE IV. Transformation properties of ferromagnetic and antiferromagnetic combinations of sublattice moments.

A_g	$M_{1z}+M_{2z}$	$(M_{1\alpha}+M_{2\alpha})^2$
	$M_{1x}-M_{2x}$	$(M_{1\alpha}-M_{2\alpha})^2$
		$(M_{1x}+M_{2x})(M_{1z}-M_{2z})$
		$(M_{1z}+M_{2z})(M_{1x}-M_{2x})$
$\underline{A}_g$	$M_{1y}-M_{2y}$	$(M_{1x}+M_{2x})(M_{1y}+M_{2y})$
		$(M_{1y}+M_{2y})(M_{1z}-M_{2z})$
		$(M_{1z}+M_{2z})(M_{1y}-M_{2y})$
		$(M_{1x}-M_{2x})(M_{1y}-M_{2y})$
B_g	$M_{1y}+M_{2y}$	$(M_{1x}+M_{2x})(M_{1y}-M_{2y})$
		$(M_{1y}+M_{2y})(M_{1z}+M_{2z})$
		$(M_{1y}+M_{2y})(M_{1x}-M_{2x})$
		$(M_{1y}-M_{2y})(M_{1z}-M_{2z})$
$\underline{B}_g$	$M_{1x}+M_{2x}$	$(M_{1x}+M_{2x})(M_{1z}+M_{2z})$
	$M_{1z}-M_{2z}$	$(M_{1x}+M_{2x})(M_{1x}-M_{2x})$
		$(M_{1y}+M_{2y})(M_{1y}-M_{2y})$
		$(M_{1z}+M_{2z})(M_{1z}-M_{2z})$
		$(M_{1x}-M_{2x})(M_{1z}-M_{2z})$

to use the tables in like manner to find the explicit forms of the second-order terms. We shall retain only those second-order terms which are no more than linear in the magnon amplitudes and also in the small quantities β and the ratio of minor to major axes of the precession ellipses of Fig. 3. With these simplifications, the magnetization-dependent part of the dielectric tensor becomes

$$\begin{aligned}
\Delta\epsilon_{xy} &= K_{xyx}(M_{1x}-M_{2x})+K_{xyz}(M_{1z}+M_{2z})+G_{xyxy}(M_{1x}-M_{2x})(M_{1y}-M_{2y}) \ , \\
\Delta\epsilon_{xz} &= K_{xzy}(M_{1y}+M_{2y})+G_{xzyx}(M_{1y}+M_{2y})(M_{1x}-M_{2x})+G_{xzxz}(M_{1x}-M_{2x})(M_{1z}-M_{2z}) \ , \\
\Delta\epsilon_{yz} &= K_{yzx}(M_{1x}+M_{2x})+K_{yzz}(M_{1z}-M_{2z})+G_{yzyx}(M_{1y}+M_{2y})(M_{1x}-M_{2x}) \\
&\quad +G_{yzxz}(M_{1x}-M_{2x})(M_{1z}-M_{2z})(M_{1z}-M_{2z}) \ ,
\end{aligned} \tag{11}$$

where the G coefficients, like the K's, describe the response of a single ion.

Let us now write these components in terms of fluctuations away from the equilibrium canted configurations. In terms of Fig. 2 (left),

$$\begin{aligned}
M_{1x} &= -M_{x'}\sin\beta + M_{z'}\cos\beta, & M_{2x} &= M_{x''}\sin\beta - M_{z''}\cos\beta \ , \\
M_{1y} &= -M_{y'}, & M_{2y} &= M_{y''} \ , \\
M_{1z} &= M_{z'}\sin\beta + M_{x'}\cos\beta, & M_{2z} &= M_{z''}\sin\beta + M_{z''}\cos\beta \ .
\end{aligned} \tag{12}$$

In linear spin wave theory the $M_{x'}$ and $M_{x''}$ components are proportional to the spin-wave amplitude while $M_{z'} = M_{z''} = M_0$, the sublattice magnetization.

Using these expressions in the dielectric function, we find, in this linear approximation,

$$\begin{aligned}
\Delta\epsilon_{xy} &= 2M_0K_{xyx}\cos\beta + 2M_0K_{xyz}\sin\beta + (K_{xyz}\cos\beta - K_{xyx}\sin\beta)(M_{x'}+M_{x''}) - 2M_0G_{xyxy}\cos\beta(M_{y'}+M_{y''}) \ , \\
\Delta\epsilon_{xz} &= K_{xzy}(M_{y''}-M_{y'}) + 2M_0G_{xzyz}\cos\beta(M_{y''}-M_{y'}) + 2M_0G_{xzxz}\cos^2\beta(M_{x'}-M_{x''}) \ , \\
\Delta\epsilon_{yz} &= (K_{yzz}\cos\beta - K_{yzx}\sin\beta)(M_{x'}-M_{x''}) + 2M_0G_{yzyx}\cos\beta(M_{y''}-M_{y'}) + 2M_0G_{yzxz}\cos^2\beta(M_{x'}-M_{x''}) \ .
\end{aligned} \tag{13}$$

The static terms in Eq. (13) are responsible for magneto-optical effects, while the terms containing $M_{x'}$, $M_{x''}$, $M_{y'}$, $M_{y''}$ give the first-order coupling to the spin-wave modes, responsible for the Raman scattering we have measured. Were the material cubic, we would have obtained only the term proportional to the net magnetization, $M_0\sin\beta$. The term $M_0\cos\beta$ is due to the lower symmetry. This enhances the magneto-optical effects as already noted by Kahn *et al.*[9] The term involving K_{yzz} in $\Delta\epsilon_{yz}$ has a similar origin.

E. Microscopic considerations

The "conventional" mechanism for one-magnon Raman scattering[10] involves the spin-orbit interaction and only occurs for one of the photon polarizations being parallel to the magnetization, i.e., through the terms $\Delta\epsilon_{yz}$ or $\Delta\epsilon_{xz}$. "Symmetric" scattering, i.e., through $\Delta\epsilon_{xy}$, arises because the axis of quantization for the orbital angular momentum and the equilibrium spin direction are not the same in the canted system. The angular momentum axis is determined by the crystalline electric fields which are, in turn, determined by the crystallographic structure. Thus, the spin-orbit interaction at site 1 takes the form

$$\begin{aligned}
\underline{H}_{s\text{-}o} &= \lambda L_x(-S_{x'}\sin\beta + S_{z'}\cos\beta) \\
&\quad -\lambda L_yS_{y'} + \lambda L_z(S_{z'}\sin\beta + S_{x'}\cos\beta) \ .
\end{aligned} \tag{14}$$

In the electric dipole approximation, the interaction with the electromagnetic field of the light has the form

$$\underline{H}_L = -e\sum_i p_\mu^{(i)}E_\mu \ , \tag{15}$$

where $p_\mu^{(i)}$ are the components of the electric moment of the ith ion. The many-electron ground state of the Fe^{3+} ion is a $^6A_{1g}$. The electric dipole transitions couple this state to a $^6T_{1u}$ consisting largely of one-electron charge-transfer transitions from the oxygen $2p$ orbitals to the iron $3d$ orbitals. Excited-state exchange will split the M_s components of the $^6T_{1u}$. Thus, the one-magnon contributions to the dielectric function $\epsilon_{\mu\nu}$ have the form

$$\frac{e^2\sum_{1,2}\left\langle {}^6A_{1g},3/2\left|\sum_i p_\mu^{(i)}\right|2\right\rangle\left\langle 2\left|H_{so}\right|1\right\rangle\left\langle 1\left|\sum_i p_\nu^{(i)}\right|{}^6A_{1g},5/2\right\rangle}{(E_0-E_1)(E_0-E_2)} \tag{16}$$

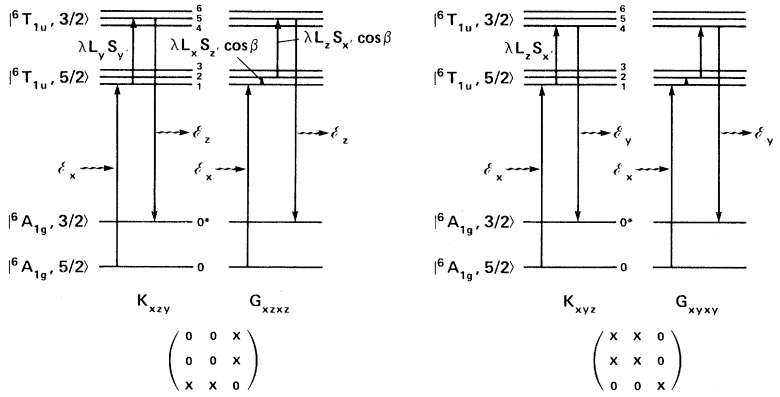

FIG. 5. Electronic energy levels associated with an Fe^{3+} ion showing the virtual transitions contributing to the two lowest-order terms in the Raman tensor.

The complete expression for $\Delta\epsilon_{\mu\nu}$ involves contributions in which μ and ν are interchanged and also in which the scattered photon is created before the incident photon is annihilated. However, Eq. (16) shows how symmetric scattering can arise. If $\nu = x$ and $\mu = y$, then states $|1\rangle$ and $|2\rangle$ have the same orbital projection numbers. Thus, $\underline{H}_{so}$ must create a spin flip without changing the orbital state. The term $\lambda L_z S_x \cos\beta$ does precisely this. Figure 5 illustrates the third- and fourth-order perturbation processes that lead to the two types of Raman scattering.

III. EXPERIMENTAL RESULTS

As mentioned in the Introduction, this study was initiated largely to measure the spin-wave frequencies of $YFeO_3$. However, a number of rare-earth orthoferrites were also measured for comparison. The samples were flux grown and most were multicrystalline with ~3-mm × 3-mm facets. The $YFeO_3$, $SmFeO_3$, and $ErFeO_3$ samples were oriented and cut along the crystallographic faces. For the other samples, spectra were obtained from several facets which appeared perpendicular. All the samples were opaque in the visible spectral region.

The Raman spectra were obtained in a near-backscatter geometry using ~200 mW of the 6471-Å line from a krypton ion laser. The laser radiation which was focused to a line image of ~3mm × 50 μm was incident at ~20° to the normal while the scattered light was collected at the normal with $f = 1.2$ optics. The incident light was polarized horizontal or vertical to the scattering plane while the scattered light was always analyzed horizontal. The scattered light was dispersed with a Spex 14018 double monochromator equipped with a third monochromator. All three monochromators were scanned simultaneously under control of a Nova 800J computer. The monochromators were stepped at 1- and 0.5-cm^{-1} intervals, and the photon counts were also stored by the computer. All the spectra presented here are raw data with straight lines drawn between data points. Peak signal count rates varied from 10 to 500 counts/sec.

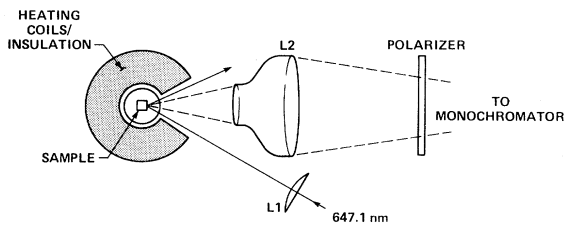

FIG. 6. Experimental arrangement used in measuring the Raman spectra at temperatures above room temperature.

To verify and examine the magnetic properties of the low-frequency excitations, the spectra of the $YFeO_3$ samples were recorded at elevated temperature using the cylindrical oven shown in Fig. 6. In addition, the oven and an immersion-type liquid-He cryostat were used to examine the spin orientation transitions in $SmFeO_3$ and $ErFeO_3$, respectively. With either the oven or the cryostat, the backscatter geometry remained unchanged. In the oven, the sample was in air, but even at temperatures above 400 °C there was no evidence of surface deterioration. All our measurements were carried out in zero magnetic field because previous Bitter pattern studies of $YFeO_3$ showed that the samples were single domain in zero field.

A. Yttrium orthoferrite

Low-frequency excitations in $YFeO_3$ were clearly observed from the c and a faces and several of the resulting spectra are shown in Figs. 7 and 8. The

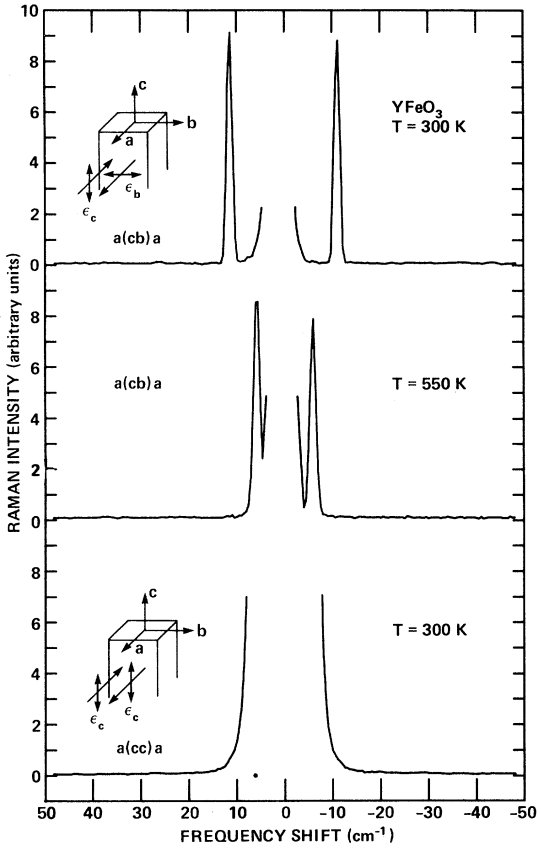

FIG. 7. Raman spectra obtained from the a face of $YFeO_3$; the notation $a(cb)a$ means that an incident light beam directed along the (negative) a-direction and polarized along the c-direction, while the scattered radiation is a polarization analyzed along the b direction and emerges along the a direction.

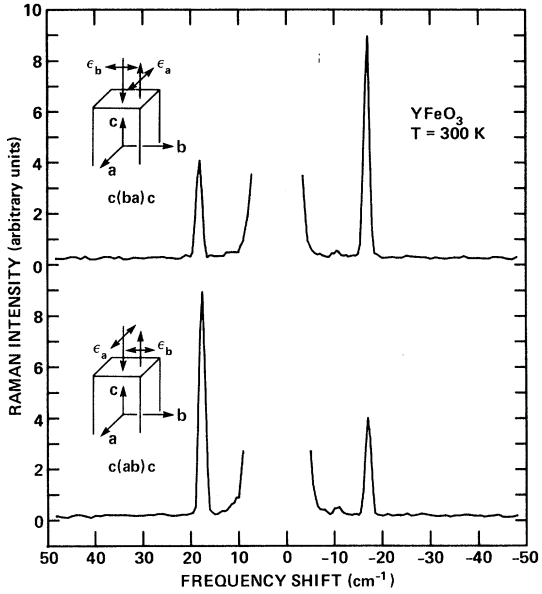

FIG. 8. Raman spectra obtained from the c face of $YFeO_3$. Both spectra were obtained in the same geometry, but but the sample was rotated by 90° around the c axis.

$c(ba)c$ spectrum showed a mode at 17 cm^{-1} while the $a(cb)a$ spectrum showed a mode at 11 cm^{-1}. Note that the spectra are associated with different Raman tensor components as predicted for the magnetic scattering. Comparison with Eqs. (8) and (9) shows that the 17-cm^{-1} mode is the γ mode while the 11-cm^{-1} mode is the σ mode. The frequencies are in reasonable agreement with the predictions. No Raman scattering could be detected from the b face, probably because of the small amplitude of the σ mode along the y' and y'' axes (see Fig. 3).

Since the index of refraction, n, of the orthoferrites is of the order of 2.3, the geometry of the scattering very nearly corresponds to that of back scattering. Thus the wave vector of the excited spinwave is approximately $2(2\pi n/\lambda)$, where λ is the laser wavelength, which, in our case, is 6471 Å. This corresponds to a spin-wave wave vector of 44.7×10^4 cm^{-1}. The freqeuencies of the spin-wave modes in this regime of small yet finite wave vectors are[2]

$$\hbar\omega_\sigma\{24JS[2(K_x-K_z)S+2JSa^2k^2]\}^{1/2}\ ,$$
$$\hbar\omega_\gamma=\{24JS[6DS\tan\beta+2K_xS+2JSa^2k^2]\}^{1/2}\ , \tag{17}$$

where a is the separation between the Fe^{3+} moments, which is 3.85 Å in the ab plane, 3.81 Å in the c direction. Using $J=20$ cm^{-1}, $D=0.88$ cm^{-1}, $\beta=8.9\times10^{-3}$ radians,[11] and the experimentally observed values for $\hbar\omega_\sigma$ and $\hbar\omega_\gamma$, we obtain $\underline{H}_{K_x}$ (defined as K_xS/μ) = 996 Oe and $H_{K_z}=245$ Oe. The in-plane anisotropy is therefore less than the reduced antisymmetric exchange field, $\underline{H}_D\tan\beta$, which is about 1250 Oe. Thus the antisymmetric exchange is the dominant factor in keeping the magnetization in the easy ac plane.

Figure 7 shows the softening of the mode as the temperature nears the Néel temperature of 645 K. Above ~600 K, the mode is no longer distinguishable from the elastically scattered light. Another experimental indication of the magnetic nature of these excitations is the linewidth. In Figs. 7 and 8, linewidths are instrumentally limited. The room-temperature measurements were repeated using spectral linewidths as small as 0.7 cm^{-1}, and the spectra were still found to be instrument limited. These narrow lines are consistent with magnetic resonance linewidths.[2]

Of particular interest is the Stokes–to–anti-Stokes (S-to-AS) intensity ratio anomaly observed in the

18-cm^{-1} mode. The S-to-AS ratio for bosons is $(\omega_S/\omega_{AS})^4 e^{\Delta\omega/kT}$ which for an 18-cm^{-1} mode at room temperature could be ~ 1. Thus the experimentally observed spectra of the 18-cm^{-1} mode are clearly inconsistent with this prediction. Even more striking is the fact that the lines reverse in intensity when the sample is rotated 90°. This corresponds to changing the Raman tensor from *ab* to *ba*. In addition, the anomaly is found to be wavelength dependent. Spectra excited at 6471 Å show a S-to-AS ratio of 2 while at 5145-Å excitation the ratio grows to ~ 3.0. In the 11-cm^{-1} mode, a variation of less than 5% was observed changing from the (*bc*) to the (*cb*) configuration. We did find, however, that the frequency shifts of the Stokes and anti-Stokes modes are identical to within our experimental accuracy of ± 0.2 cm^{-1}.

This anomaly in the S-to-AS ratio has been observed in other systems and has been attributed[12,13] to an interference between one-magnon terms arising from the linear magnetic (K) contributions to the dielectric function and those arising from quadratic contributions (G). We shall illustrate this for the case of $c(ba)c$ or $c(ab)c$ scattering by the γ mode (Fig. 8). This scattering is induced by the magnon modulation of the component ϵ_{xy} of the dielectric function. To leading order (i.e., with $\beta \to 0$), we can use (13) to express the oscillating part of ϵ_{xy} in terms of the magnon creation and destruction operators γ^+, γ:

$$\begin{aligned}\Delta\epsilon_{xy}(\text{osc.}) &= K_{xyz}(M_{x'}+M_{x''}) \\ &\quad -2M_0 G_{xyxy}(M_{y'}+M_{y''}) \\ &\propto (irK_{xyz}+2G_{xyxy})\gamma \\ &\quad -(irK_{xyz}-2G_{xyxy})\gamma^+ , \end{aligned} \tag{18}$$

where r is the ratio of the minor to major axes of the ellipse generated by transverse components of the precessing magnetization, as shown in Fig. 3. Since both K and G are complex, the S-to-AS ratio (I) becomes

$$I=\left[\frac{(rK'_{xyz}+2G''_{xyxy}M_0)^2+(rK''_{xyz}-2G'_{xyxy}M_0)^2}{(rK'_{xyz}-2G''_{xyxy}M_0)^2+(rK''_{xyz}+2G'_{xyxy}M_0)^2}\right]\left[\frac{n_\gamma+1}{n_\gamma}\right] . \tag{19}$$

When $\hbar\omega_\gamma \ll k_B T$, the thermal factor $(n_\gamma+1)/(n_\gamma)$ can be neglected. Figure 9 shows the real and imaginary parts of K_{xyz}.[9] At the longer wavelength used, the crystal is not very absorptive, i.e., K'_{xyz} is small. If we also assume G is Hermitian, then the first terms in the numerator and denominator of (19) can be neglected, and a S-to-AS ratio of 2 implies $2G'_{xyxy}M_0$ is 20% of rK''_{xyz}. Notice that the ellipticity r of the γ mode enhances this interference effect. In the case of the σ mode, the ellipticity enters in the opposite way (multiplying the G tems instead of the K terms), thereby suppressing the interference.

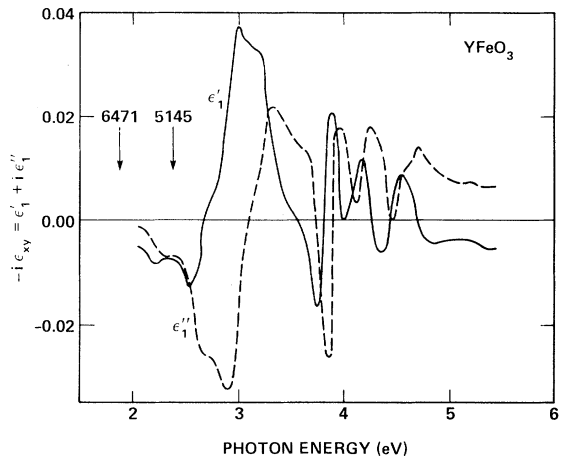

FIG. 9. Real and imaginary parts of the off-diagonal element of the dielectric function as functions of frequency (Ref. 9); the two wavelengths indicated refer to the two excitation wavelengths used in this study.

Rotating the sample by 90° changes the sign of K''_{xyz}, which is antisymmetric, but does not affect G'_{xyxy}, which is symmetric. This clearly inverts the ratio, and accounts for the experimental observation.

B. Rare-earth orthoferrites

At room temperature, the Fe^{3+} sublattices in the three rare-earth orthoferrites $DyFeO_3$, $HoFeO_3$, and $ErFeO_3$ have the same orientation as in $YFeO_3$. The Fe^{3+}-Fe^{3+} exchange interactions are still the dominant interactions in these materials as witnessed by the fact that their Néel temperatures are close to those of $YFeO_3$. However, at lower temperatures, the iron sublattices in $HoFeO_3$ and $ErFeO_3$ undergo a 90° reorientation in the *ac* plane. This configuration, illustrated in Fig. 2 (right), is denoted $\Gamma_2(F_x)$. Samarium orthoferrite differs from these orthoferrites in that its spin reorientation temperature is above room temperature, which means that its spin configuration at room temperature is $\Gamma_2(F_x)$.

The room-temperature Raman spectra of these materials are shown in Fig. 10 along with $YFeO_3$ for comparison. The frequencies of the modes are listed in Table V. The scattering at 18 cm^{-1} in $SmFeO_3$ was seen only on the *b* face and is very weak, showing a peak intensity of 10 counts/sec. This is 10 to 100 times weaker than the other materials. We associate this scattering with the γ mode. The σ mode at 9 cm^{-1} was observed from all three faces, although most strongly from the *c* face. The observed scattering intensities of the Raman tensor components for

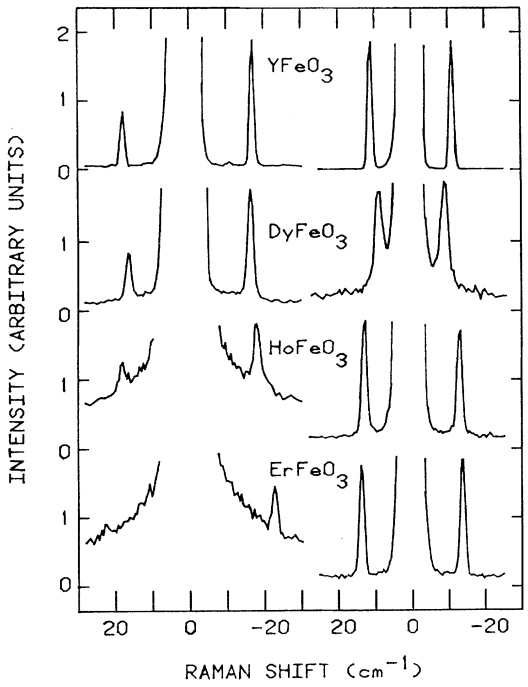

FIG. 10. Raman spectra of several rare-earth orthoferrites at room temperature; the left column corresponds to scattering from the c face, i.e., $c(ab)c$, while the right column corresponds to $a(cb)a$.

$YFeO_3$ (Γ_4) and $SmFeO_3$ (Γ_2) are summarized in Table VI. The fact that the γ mode is seen only on the b face rather than the a face, as we might have expected from our results on the other orthoferrites, suggests that microscopic considerations favor the corresponding K coefficient in an expansion analogous to Eq. (13).

TABLE V. Room-temperature frequencies of γ and σ modes.

Material	Magnetic configuration	σ	γ
$YFeO_3$	$\Gamma_4(F_z)$	11.1	17.4
$DyFeO_3$	$\Gamma_4(F_z)$	9.1	16.5
$HoFeO_3$	$\Gamma_4(F_z)$	13.0	18.0
$ErFeO_3$	$\Gamma_4(F_z)$	13.75	22.7
$SmFeO_3$	$\Gamma_2(F_x)$	8.9	18.4

TABLE VI. Summary of the intensities of the components of the Raman tensor R [see Eqs. (8) and (9)] observed in $YFeO_3$ and $SmFeO_3$ at room temperature (VS = very strong, S = strong, M = medium, W = weak, VW = very weak).

	9,11 cm^{-1}			18 cm^{-1}		
	0	0	0	0	S	0
$YFeO_3$	0	0	VS	S	0	0
	0	VS	0	0	0	0
	M	S	W	0	0	VW
$SmFeO_3$	S	M	W	0	0	0
	W	W	0	VW	0	0

C. Spin reorientation

1. Results

The reorientation region causes striking effects in the Raman spectra. Since the light scattering is sensitive to the small-k excitations, any mode softening will be observed and, in addition, in the reorientation region, the magnon modes transform as linear combinations of the respective representations of the $\Gamma_4(F_z)$ and $\Gamma_2(F_x)$ space groups. Thus the modes should be observed in several scattering geometries.

Consider first the $ErFeO_3$ (Fig. 11). At room temperature this material exhibits $\Gamma_4(F_z)$ symmetry, and σ mode is observed from the b face only while the γ mode is observed only from the c face. As the temperature is lowered from room temperature, the intensity of the modes decreases gradually, consistent with a normal dependence for scattering from boson excitations [i.e., for Stokes scattering, $I \propto [n(\omega)+1]$]. The frequency of the γ mode remains constant while the σ mode frequency decreases as the temperature is lowered. We note that this decrease in frequency is contrary to expected behavior for a simple ferro- (or anti-ferro-) magnetic system. This effect is suggestive of a phase transition.

The temperature dependence of the frequencies and intensities of the $ErFeO_3$ magnon modes is summarized in Fig. 11. First, we note that the γ and σ modes are both observed from the c face in the reorientation region. The frequency of the γ mode is independent of the reorientation; however, the σ-mode frequency is certainly affected. At the high-temperature limit of the transition, only the rate of softening seems to change while, at the low-temperature limit, a slight dip in frequency is observed. A relatively rapid increase of frequency is noted as the temperature decreases, where a value of 19.2 cm^{-1} was found at ~8 K. As has been shown by Koshizuka and Ushioda,[14] the intensity dependence most clearly

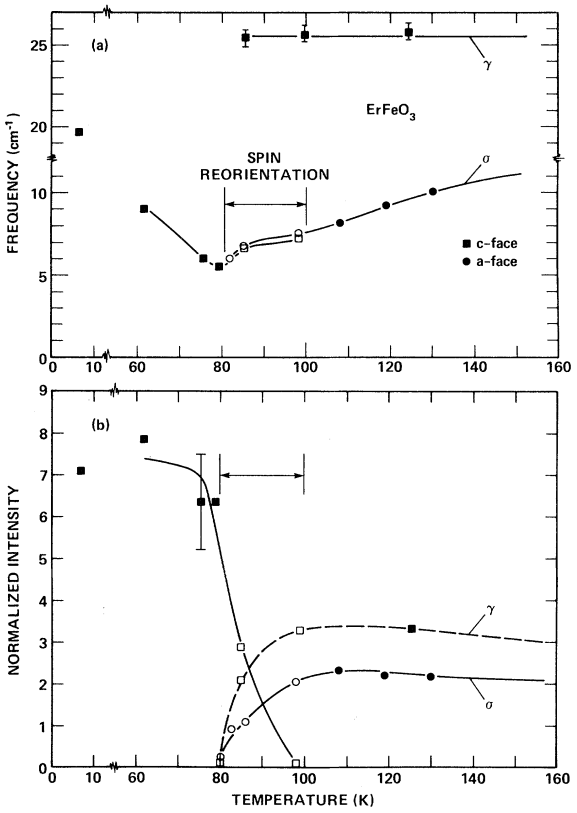

FIG. 11. (a) Frequency dependence and (b) normalized intensity dependence of the σ and γ modes in $ErFeO_3$ as a function of temperature. The Stokes peak intensity has been normalized by $(n+1)/\omega$.

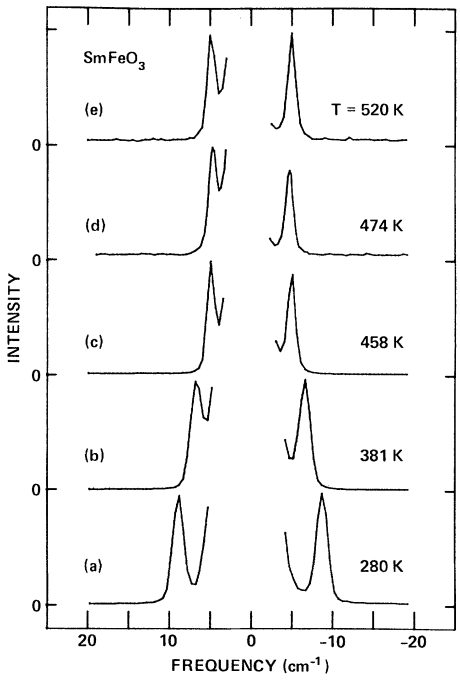

FIG. 12. (a)–(e) Raman spectra of $SmFeO_3$ at various temperatures.

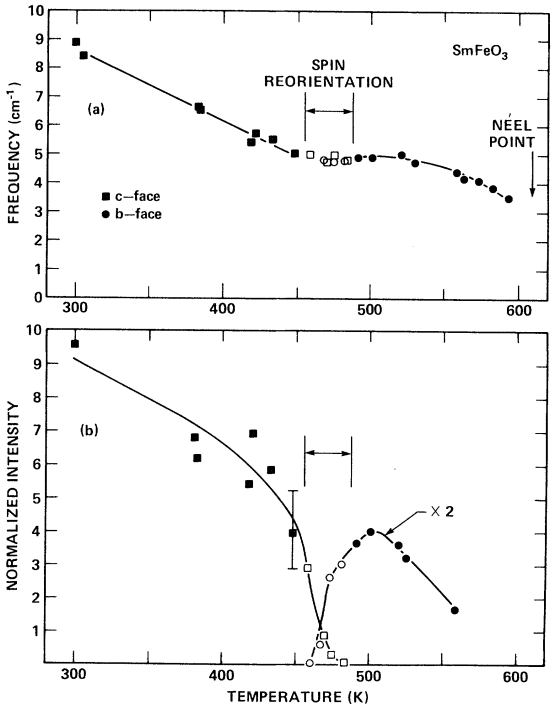

FIG. 13. (a) Frequency dependence and (b) normalized intensity dependence of σ mode in $SmFeO_3$ as a function of temperature. The Stokes peak intensity has been normalized by $(n+1)/\omega$.

defines the transition region. For light scattering from sharp boson excitations, the light scattering intensity is proportional to $[n(\omega)+1]/\omega$. Thus, to ascertain the temperature dependence of the light scattering matrix element, we have normalized our measured peak intensity by this term. Here the measured frequency and temperature were used. We see from Fig. 11(b) that, away from the transition, the intensity is relatively constant, but through the transition the intensity changes are significant. Here, for the σ mode, the drop in intensity for scattering from the a face was matched by an increase in intensity of the corresponding feature from the c face. The γ-mode intensity decrease parallels that of the σ mode but was unobserved below the transition. This observation is consistent with the room-temperature measurements of $SmFeO_3$ [$\Gamma_2(F_x)$], where the γ mode was exceptionally weak. The Raman results shown here are similar to those that have been recently published by Koshizuka and Ushioda[14] and also consistent with the neutron scattering results.[15]

Consider now the $SmFeO_3$. This material exhibits

a spin reorientation in the temperature range ~460 to 480 K. A series of representative spectra of the σ mode is shown in Fig. 12. The behavior of the frequencies and intensities are summarized in Fig. 13. There are both similarities and notable differences between the transitions of the two materials. In the $SmFeO_3$, there is no dip at the lower-temperature limit of the transition, but a definite change of slope of the frequency as a function of temperature is observed. In addition, the upper-temperature limit of the transition shows no observable effect in the frequency dependence. As the "Néel" point is approached, the expected softening is observed. This temperature dependence is to be contrasted with the $ErFeO_3$, where the frequency rises significantly for temperature increasing above the transition. The intensity behavior is most similar for both materials and again serves as a demarcation of the reorientation transition. As mentioned earlier, the γ mode is exceptionally weak in the $SmFeO_3$ at room temperature, and, in the oven configuration, we were not able to observe it. We attempted to note its presence in the high-temperature phase, and again it was still unobservable.

2. *Discussion*

The spin reorientation has been extensively studied and ascribed to various mechanisms. One of these[16] argues that the anisotropy parameters K_X and K_Z in (6) are temperature dependent, with the difference $K_X - K_Z$ changing sign at a temperature near the middle of the range where the spin reorientation is observed. Near this temperature, $K_X - K_Z$ is small, and, for an adequate description of the variation of free energy with spin orientation, it is necessary to retain the small fourth-order anisotropy term. This model predicts that, if the sign of the fourth-order anisotropy term is such as to make it a maximum when the ferromagnetic moment $M = M_1 + M_2$ points along the a and c axis, and a minimum at 45°, then with increasing temperature the equilibrium direction of M will start at some temperature T_1 to rotate away from the a direction toward the c, and will reach the latter at a higher temperature, T_2. At both temperatures, T_1 and T_2, the frequency of the $k = 0$ σ mode will vanish, but at intermediate temperatures it will be finite. Although this predicted behavior of the mode frequency has received only partial confirmation in the literature, the model was widely accepted for some years, and some of its other predictions accord nicely with observations,[17] especially for spin-reorientation transitions in mixed crystals without rare-earth spins.[18] As we have just seen, our Raman results show no sign of mode softening for $SmFeO_3$, and only a slight softening (at the lower transition temperature) for $ErFeO_3$, our result for the latter material being similar to that obtained by neutron scattering.[15]

In more recent years, a number of workers have espoused the view that the transitions in orthoferrites with unfilled f shells are primarily due to the coupling of the iron and rare-earth spins.[19–22] For one thing, they do not occur when the rare-earth ion has no spin (Y, La, Lu) or a $J = 0$ ground state (Eu).[1] Also, the rare-earth magnetization, with its T^{-1} variation at high temperatures, provides a natural source for temperature-dependent terms in the free energy. The most detailed analysis of the role of rare-earth spins in spin-reorientation transitions seems to be that of Yamaguchi,[19] who employed a free-energy expression dependent on the orientations of four iron sublattices and four rare-earth sublattices, with isotropic, anisotropic, and antisymmetric exchange couplings, and with the magnitude of the magnetization of a rare-earth sublattice as a temperature-dependent parameter. However, the magnon modes of a system of coupled iron and rare-earth sublattices have been much less carefully studied; an early paper by Aring and Sievers[20] quoted some results that were used to interpret optical absorption data on $YbFeO_3$ near its low-temperature spin reorientation at ~8 K, but used a model appropriate only near the high-temperature spin configuration, $\Gamma_4(F_Z)$. So until a more complete analysis of such modes is available, our discussion of the role of rare-earth spins in the interpretation of our experimental results must be somewhat tentative.

One simple fact, applicable to essentially any model of the magnon modes, must be borne in mind: part of the reason that we do not observe a complete softening of the spinwave is that Raman scattering involves modes of finite wavevector. In Fig. 14, we plot the spectrum for the σ mode, as obtained for a simple model with two iron sublattices,[2] for a typical value of $K_X - K_Z$ and also for $K_X - K_Z = 0$. The curvature of the upper plot, drawn for a temperature

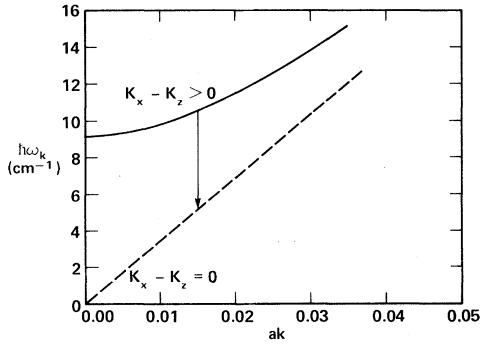

FIG. 14. Small wave-vector dependence of the σ mode for a typical value of $K_X - K_Z$ (solid curve) and at the soft-mode condition (dashed line).

well away from the spin reorientation, is determined by the relative magnitudes of the anisotropy $(K_X - K_Z)$ and exchange (J) energies, and is reasonably known. The wave vector of the mode excited is $2n = 4.6$ times that of the photon in air, where n is the refractive index, and turns out to correspond to $ak = 0.015$, a value that is not negligible on the scale of the figure. If the mode were to soften completely at $k = 0$, as shown in the dashed curve, we would expect only about a 50% reduction in the frequency. But this does not suffice to explain our $SmFeO_3$ results. Nor does it explain the neutron results on $ErFeO_3$, which do measure the $k = 0$ frequency.

Thus it is tempting to conclude that, especially in $SmFeO_3$, the coupling of the iron spins to the weakly but appreciably magnetized rare-earth sublattices is preventing the σ-mode frequency from softening very markedly at $k = 0$. The essential physics involved is probably contained in the Aring-Sievers model mentioned above,[20] which postulated two iron sublattices with a Hamiltonian of the form (6) plus a small canting-anisotropy term involving products $\vec{S}_i \times \vec{S}_j$, and two rare-earth sublattices coupled to the iron by an exchange Hamiltonian H' with a large antisymmetric component:

$$\underline{H}' = 2J \sum_{i,\delta} \vec{S}_i \cdot \vec{R}_{i+\delta} + 2 \sum_{i,\delta} \vec{d} \cdot \vec{R}_{i+\delta} \times \vec{S}_i \ , \qquad (20)$$

where $\vec{R}$ is the rare-earth moment. They calculated the magnetic excitation spectrum, consisting of four mode branches. Two of these, which they denoted ω_f and ω_+, correspond to our γ and σ modes, respectively, while the other two, denoted ω_R and ω_-, correspond to rare-earth excitations; of course, the coupling [Eq. (20)] causes some rare-earth motion in the former modes, and some iron motion in the latter. The mode ω_R has no dispersion and corresponds to the frequency of a single rare earth in the exchange field of the iron sublattices. The ω_- mode is strongly dependent on the rare-earth magnetization; at a certain value of the latter, the effect of the iron anisotropy in (6) is cancelled and the frequency $\omega_- \to 0$. Thus, the resistance of the entire spin system to reorientation disappears. The spin-wave mode ω_+, however, remains relatively unchanged. One thus expects the behavior shown schematically in Fig. 15. When the ω_- frequency goes to zero at $k = 0$, the respective eigenstate corresponds to a rotation of the whole spin system (both irons and rare earths), but the ω_+ mode for the same set of conditions may be only slightly softened, and its motion may continue to involve predominantly precessions of the iron spins. In such case, the ω_+ mode will couple in Raman scattering very much as it does far from the spin-reorientation transition. Moreover, it seems possible that, for quite a range of parameter values, the frequency of the σ mode can

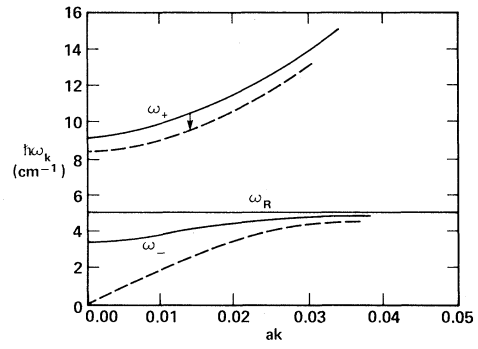

FIG. 15. Magnetic excitations in a rare-earth orthoferrite with an exchange-split Kramers doublet; dashed curves correspond to the point at which the rare-earth–iron exchange just cancels the iron anisotropy. The uppermost mode, ω_f, is not shown.

be almost the same on both sides of the spin-reorientation transition.

Although the Aring-Sievers model omits many features characteristic of real rare-earth orthoferrites, notably anisotropy energies of the rare-earth spins,[23] it is not unreasonable to expect in most cases a behavior similar to that just outlined. This would be natural for odd-electron systems where the rare-earth ground state will be an exchange-split Kramers doublet. In $ErFeO_3$, for example, optical spectroscopy[24] shows that the Er^{3+} ground state is split by 3 cm^{-1} at 77 K. Similarly, the infrared absorption studies[20] on $YbFeO_3$ suggest a rare-earth exchange splitting of 5 cm^{-1}. In even-electron systems, however, the possibility of relatively widely spaced electronic singlets should be considered. In $TmFeO_3$, the lowest two singlets are separated[25,26] by 17.5 cm^{-1}. This means the spin waves lie below the rare-earth excitations, and we might expect the more familiar soft-mode behavior as, indeed, the neutron data[15] seem to indicate. However, in several other cases,[26,27] it seems that there is a ground pair of closely spaced crystal-field singlets, separated by some tens of wave numbers from the higher levels. In such cases, when there is a nonvanishing matrix element of the moment between the two states, the ground pair can again behave like an orientable spin.

To sum up, we believe that our failure to observe significant softening of the σ mode of $SmFeO_3$ at either end of the spin-reorientation transition implies that the parameters of the coupled iron–rare-earth system are such that the corresponding mode softens only slightly at these temperatures, although the frequency of a lower-lying mode does indeed go to zero. For $ErFeO_3$, the σ-mode softening is perceptible, though again not complete. The contrast we find between $TmFeO_3$ and $ErFeO_3$ is similar to that noted in neutron depolarization by Baazov *et al.*[28]

ACKNOWLEDGMENTS

We are grateful to J. Zesch for orienting and polishing the samples used in this study, and to R. L. White for several suggestions.

APPENDIX

In this Appendix, we derive relations that describe how a response function transforms under symmetry operations that include products of time reversal with spatial transformations, i.e., RT, as well as spatial transformations alone, S.

The general expression for a response function involving the operators A and B is

$$X_{AB}(t) = \sum_n \langle n|\rho_0[A(t,H),B]|n\rangle \ , \tag{A1}$$

where $A(t,H) = \exp(iHt)A\exp(-iHt)$. The density matrix ρ_0 reflects the symmetry of the system, i.e.,

$$R^{-1}T^{-1}\rho_0 RT = S^{-1}\rho_0 S = \rho_0 \ . \tag{A2}$$

Using the time reversal property

$$\langle\psi|\varphi\rangle = \langle T\psi|T\varphi\rangle^* \ ,$$

the response function may be written

$$X_{AB}(t) = \sum_n \langle RTn|RT\rho_0[A(t,H),B]R^{-1}T^{-1}|RTn\rangle^* \ . \tag{A3}$$

We now use the fact that ρ_0 commutes with RT and recognize that, since the sum runs over all states, we may write $RTn \equiv m$ and then change $m \rightarrow n$. Thus,

$$X_{AB}(t) = \sum_n \langle\{\rho_0 RT[A(t,H),B]R^{-1}T^{-1}\}n|n\rangle \tag{A4}$$

$$= \sum_n \langle\{\rho_0[A_{RT}(-t,H),B_{RT}]\}n|n\rangle \ , \tag{A5}$$

where $A_{RT} \equiv RTAR^{-1}T^{-1}$ and H is the time-reversed Hamiltonian. We shall assume that H is invariant under time reversal. Thus

$$X_{AB}(t) = \sum_n \langle n|[B_{RT}^+, A_{RT}^+(-t,H)]\rho_0|n\rangle \ . \tag{A6}$$

In most cases, A and B will be Hermitian operators. If ρ_0 commutes with H then

$$X_{AB}(t) = \sum_n \langle n|\rho_0[B_{RT}(t,H),A_{RT}]|n\rangle \ . \tag{A7}$$

Let us now consider the case where the representations of the group we are considering are all one dimensional, and that A transforms according to the representation D_A and B according to D_B. Then

$$B_{RT} = \theta(RT)_{D_B} B \ ,$$

and

$$A_{RT} = \theta(RT)_{D_B} A \ ,$$

where the $\theta(RT)_{D_B}$, for example, is the character associated with the operation RT in the representation D_B. Then the response function satisfies

$$X_{AB}(t) = \theta_{D_A}(RT)\theta_{D_B}(RT)X_{BA}(t) \ . \tag{A8}$$

For those operations not involving time reversal, we obtain directly from line (A3)

$$X_{AB}(t) = \theta_{D_A}(S)\theta_{D_B}(S)X_{AB}(t) \ . \tag{A9}$$

Let us now use these relations to derive the symmetry properties of the various components of the dielectric tensor.

For the diagonal components the products of the characters in Eqs. (A8) and (A9) are all $+1$. Thus, the diagonal components must all transform according to the representation A_g.

Now consider ϵ_{xy}. Equation (A8) tells us that $\epsilon_{xy} = -\epsilon_{yx}$ for all RT, while Eq. (A9) gives $\epsilon_{xy} = \epsilon_{xy}$ for all S. Since $[\epsilon_{yx}^H]'' = -[\epsilon_{xy}^H]''$ and $[\epsilon_{yx}^A]' = -[\epsilon_{xy}^A]'$, these relations imply that $[\epsilon_{xy}^H]''$ and $[\epsilon_{xy}^A]'$ must transform like A_g. Similarly, we see that $[\epsilon_{xy}^H]'$ and $[\epsilon_{xy}^A]''$ must transfrom like $\underline{A}_g$. In Table III, we list the symmetries of the various components.

---

*Also at the Department of Applied Physics, Stanford University, Stanford, Cal. 94305.

[1]For a review of the rare-earth orthoferrites, see R. L. White, J. Appl. Phys. 40, 1061 (1969).
[2]Ching H. Tsang, Robert L. White, and Robert M. White, J. Appl. Phys. 49, 6052, 6063 (1978).
[3]R. M. White, R. J. Nemanich, and C. Tsang, J. Magn. Magn. Mater. 15–18, 773 (1980).
[4]S. Geller and E. A. Wood, Acta Crystallogr. 9, 563 (1956).
[5]See, for example, Arthur P. Cracknell, Prog. Theor. Phys. 35, 196 (1966).
[6]E. Wigner, *Group Theory and Its Application to Quantum Mechanics of Atomic Spectra* (Academic, New York, 1959).
[7]Gabriel F. Herrmann, Phys. Rev. 133, A1334 (1964).
[8]A. P. Cracknell, J. Phys. C 2, 500 (1969).
[9]Frederic J. Kahn, P. S. Pershan, and J. P. Remeika, Phys. Rev. 186, 891 (1969).
[10]P. A. Fleury and R. Loudon, Phys. Rev. 166, 514 (1968).
[11]D. Treves, Phys. Rev. 125, 1843 (1962); J. Appl. Phys. 36, 1033 (1965).

[12]H. LeGall, Tran Khanh Vien, and B. Desormiere, Phys. Status Solidi 47, 591 (1971).
[13]W. Wettling, M. G. Cottam, and J. R. Sandercock, J. Phys. C 8, 211 (1975).
[14]N. Koshizuka and S. Ushioda, Phys. Rev. B 22, 5394 (1980).
[15]S. M. Shapiro, J. D. Axe, and J. P. Remeika, Phys. Rev. B 10, 2014 (1974).
[16]J. R. Shane, Phys. Rev. Lett. 20, 728 (1968); F. B. Hagedorn and E. A. Gyorgy, Phys. Rev. 174, 540 (1968).
[17]See, for example, the review by K. P. Belov, A. K. Zvezdin, A. M. Kadomtseva, and R. Z. Levitin, Usp. Fiz. Nauk 119, 447 (1976) [Sov. Phys. Usp. 19, 574 (1976)].
[18]L. Holmes, L. G. Van Uitert, and R. R. Hecker, J. Appl. Phys. 42, 657 (1971); A. M. Kadomtseva, A. S. Moskvin, I. G. Bostrem, B. M. Wanklyn, and N. A. Khatizova, Zh. Eksp. Teor. Fiz. 72, 2286 (1977) [Sov. Phys. JETP 45, 1202 (1977)].
[19]T. Yamaguchi, J. Phys. Chem. Solids 35, 479 (1974).
[20]K. B. Aring and A. J. Sievers, J. Appl. Phys. 41, 1197 (1970); K. B. Aring, thesis (Cornell University, 1970) (unpublished).
[21]A. S. Moskvin, Fiz. Tverd. Tela (Leningrad) 20, 3152 (1978) [Sov. Phys. Solid State 20, 1819 (1978)].
[22]A. K. Zvezdin and V. M. Matveev, Zh. Eksp. Teor. Fiz. 77, 1076 (1979) [Sov. Phys. JETP 50, 543 (1979)]; K. P. Belov, A. K. Zvezdin, A. M. Kadomtseva, I. B. Krynetskii, and V. M. Matveev, Fiz. Tverd. Tela (Leningrad) 19, 259 (1977) [Sov. Phys. Solid State 19, 149 (1977)].
[23]In some cases, the rare-earth spin seems to have almost an Ising character: I. Nowick and H. J. Williams, Phys. Lett. 20, 154 (1966); see also Ref. 22.
[24]R. Faulhaber, S. Hüfner, E. Orlich, and H. Schuchert, Z. Phys. 204, 101 (1967); D. L. Wood, L. M. Holms, and J. P. Remeika, Phys. Rev. 185, 689 (1969).
[25]A. P. Malozemoff, J. Phys. Chem. Solids 32, 1669 (1971).
[26]J. Rossat-Mignod and F. Tcheou, J. Phys. (Paris) 33, 423 (1972).
[27]J. C. Walling and R. L. White, Phys. Rev. B 10, 4737 (1974).
[28]N. G. Baazov, E. A. Biryukova, Yu. M. Kolesnikov, M. M. Lukina, and S. I. Shilo, Fiz. Tverd. Tela (Leningrad) 18, 1390 (1976) [Sov. Phys. Solid State 181, 801 (1976)].